The FASEB Journal express article 10.1096/fj.01-0925fje. Published online April 10, 2002.

Evidence of Connective Tissue Involvement in Acupuncture

Helene M. Langevin*, David L. Churchill*, Junru Wu[†], Gary J. Badger[§], Jason A. Yandow*, James R. Fox[‡], and Martin H. Krag[‡]

*Departments of Neurology, [†]Physics, [‡]Orthopaedics and Rehabilitation, and [§]Medical Biostatistics, University of Vermont College of Medicine, Burlington, Vermont

Corresponding author: Helene M. Langevin, Department of Neurology, Given C423, University of Vermont College of Medicine, Burlington VT 05405. E-mail: hlangevi@zoo.uvm.edu

ABSTRACT

Acupuncture needle manipulation gives rise to "needle grasp," a biomechanical phenomenon characterized by an increase in the force necessary to pull the needle out of the tissue (pullout force). This study investigates the hypothesis that winding of connective tissue, rather than muscle contraction, is the mechanism responsible for needle grasp. We performed 1) measurements of pullout force in humans with and without needle penetration of muscle; 2) measurements of pullout force in anesthetized rats, with and without needle rotation, followed by measurements of connective tissue volume surrounding the needle; 3) imaging of rat abdominal wall explants, with and without needle rotation, using ultrasound scanning acoustic microscopy. We found 1) no evidence that increased penetration of muscle results in greater pullout force than increased penetration of subcutaneous tissue; 2) that both pullout force and subcutaneous tissue volume were increased by needle rotation; 3) that increased periodic architectural order was present in subcutaneous tissue with rotation, compared with no rotation. These data support connective tissue winding as the mechanism responsible for the increase in pullout force induced by needle rotation. Winding may allow needle movements to deliver a mechanical signal into the tissue and may be key to acupuncture's therapeutic mechanism.

Key Words: biomechanics • subcutaneous tissue • mechanical stress • ultrasound • histology

An important issue facing the medical and scientific community is whether or not to endorse the practice of "alternative" therapies used by a substantial percentage of the population (1). A problem inherent to this issue is that many such therapies claim to be based on phenomena that lay outside our current understanding of physiology. The objective investigation of such phenomena is therefore important to either establish or refute these claims. If these phenomena are not substantiated, this will discourage the practice of treatments based on false assumptions. However, if these phenomena can be measured and studied objectively, their understanding may lead to important new insights into some basic physiological or therapeutic mechanisms.

Acupuncture has been practiced in China for more than 2000 years (2, 3) and has become increasingly popular in the Western world. Although acupuncture is one of the alternative

therapies that have been the most studied over the past 20 years, much remains unknown regarding the mechanisms that might lead to its therapeutic effect (4). A phenomenon linked to acupuncture, which so far has remained unexplained, is the characteristic reaction to needling known as “de qi” (3). De qi is widely considered essential to acupuncture’s therapeutic effect (3, 5–7). De qi includes a sensory component experienced by the patient as an aching sensation in the area of the needle. Simultaneously with this needling sensation, the acupuncturist feels as if the tissue is contracting around the needle, such that there is increased resistance to further motion of the needle (3, 5, 8–10). We refer to this biomechanical component of de qi as “needle grasp”.

Needle grasp can be quantified objectively by measuring the amount of force necessary to pull the acupuncture needle out of the skin (pullout force) (11). Manual manipulation of the needle (e.g., rotation, pistoning) is used clinically to enhance needle grasp (3). Using a programmable robotic acupuncture needling instrument, we have shown that needle rotation markedly increases pullout force (11). Indeed, pullout forces of up to 4.9 N (equivalent to the weight of a 500 g mass) were measured after needle rotation. Needle grasp is therefore a measurable biomechanical phenomenon associated with acupuncture needle manipulation.

A frequently quoted physiological explanation for needle grasp is that it is due to a contraction of skeletal muscle (7, 12, 13). However, this theory has not been supported by quantitative data. As an alternative to this explanation, we have previously hypothesized a different and novel mechanism for needle grasp involving connective tissue rather than muscle (14). We proposed that winding connective tissue during needle rotation creates a tight mechanical coupling between needle and tissue, which allows needle manipulation to deliver a powerful mechanical signal into the tissue. This hypothesis was supported by histological observations in rat tissue explants that showed marked thickening of subcutaneous tissue and a whorl of dense connective tissue around the needle with needle rotation (14). We also hypothesized that downstream effects of mechanical signal transduction, including changes in gene expression and extracellular matrix composition, may explain local and remote as well as long-term effects of acupuncture.

In this study, we have used three complementary experimental approaches to test the first step of the above hypothesis: that the increase in pullout force with needle rotation results from winding of connective tissue, rather than contraction of muscle. First, we examined the role played by muscle versus connective tissue in needle grasp; we measured pullout force in healthy human subjects with and without needle penetration of muscle, while controlling for depth of needle insertion. Second, we examined the effect of needle rotation on both pullout force and subcutaneous tissue thickness in the area of the needle; we measured pullout force in live anesthetized rats, with and without needle rotation, followed by rapid tissue fixation and measurement of dense connective tissue volume in serial-sectioned histological specimens. Finally, we examined the effect of needle rotation on the architectural pattern of subcutaneous tissue; we used high frequency (50 MHz) ultrasound scanning acoustic microscopy to obtain high-resolution images of rat abdominal wall tissue explants with and without needle rotation. Based on previous histological observations suggesting a spiral pattern in the tissue with needle rotation, we hypothesized that the pattern in the acoustic image generated by the main components of subcutaneous connective tissue (collagen, elastic fibers, fat, extracellular matrix)

shows increased periodic order after acupuncture needle rotation, compared with needle insertion without rotation.

METHODS

Human subject protocol

This experiment was part of a study of 60 healthy human subjects aged 18–55 approved by the University of Vermont Institutional Review Board. Exclusion criteria and subject characteristics were described previously (11). Because acupuncture is practiced by using various needle manipulation methods, we tested three types of needle manipulation: bi-directional rotation (BI), uni-directional rotation (UNI), and needle insertion with no rotation (NO). After obtaining informed consent, subjects were randomized into one of three groups (NO, BI, and UNI), which differed only in the type of manipulation used. Each subject participated in one testing session, during which 10 different sites on the body received acupuncture needling bilaterally. Eight of these sites (on arms and legs) were used for comparing traditional "acupuncture points" with "non-acupuncture" control points (see ref 11 for previously published results). The two remaining locations (on the lower back, lumbar, and sacral) were used for the current study. These two locations were marked bilaterally with a skin marker: the lumbar location at the level of the L2-3 interspace, 5 cm lateral to the midline, and the sacral location at the level of the S1 sacral foramen, 10 cm lateral to the midline.

The goal of this experiment was to determine whether muscle or subcutaneous tissue is responsible for needle grasp. We took advantage of the greater subcutaneous tissue thickness present, in the vast majority of subjects, in the sacral compared with the lumbar area. Within subjects and for each location (lumbar and sacral), right and left sides of the body were assigned randomly to two different needle depths (D and D+1). D was defined as the thickness of subcutaneous tissue at the lumbar location determined by ultrasound, and D+1 was equal to D plus 1 cm (Fig. 1a). Ultrasound imaging was performed with an Acuson 128 ultrasound machine (Acuson, Mountain View, CA) equipped with a 7 MHz linear array transducer held perpendicular to the skin. With ultrasound imaging, the perimuscular fascia is visible as an echogenic line separating two tissues of different echogenicity and compressibility (subcutaneous tissue vs. muscle). In preliminary testing, we found close agreement (within 1 mm) between ultrasound identification of perimuscular fascia compared with electromyographic determination of muscle insertional activity. In all subjects, subcutaneous tissue thickness was at least 1 cm greater at the sacral than at the lumbar location. Both sacral needles (S_D, S_{D+1}) thus were inserted into skin and subcutaneous tissue only, whereas one of the lumbar needles (L_{D+1}) was inserted 1 cm into muscle. Subjects were not told, nor were they able to see or hear, which needle depth or which needle manipulation type was being performed throughout the testing.

Human acupuncture needling procedure and pullout force measurements

Acupuncture needle insertions, manipulations, and pullout force measurements were performed by using a computer-controlled acupuncture needling instrument as previously described (11). The number of needle revolutions was 16 clockwise for UNI, 16 alternating clockwise and

counterclockwise cycles of 4 revolutions each for BI, and 0 for NO. All other needling parameters, with the exception of needle insertion depth (see above), were held constant across all points and all subjects: needle insertion speed was 10 mm/s; rotation speed was 8 revolutions/second; needle dwell time was 2 s before manipulation and 10 s following manipulation; pullout speed was 5 mm/s. These parameters were determined by observing and simulating needle manipulations performed by a trained acupuncturist (H. M. Langevin).

In vivo rat pullout force and connective tissue volume measurements

All procedures were approved by the University of Vermont Animal Care and Use Committee. Thirteen normal male Sprague Dawley rats (250–275g) were anesthetized with isoflurane (2%). An acupuncture needle (Seirin, Japan, 40 mm in length and 0.25 mm in diameter) was inserted on both sides of the abdomen at the midaxillary line, midway between the lower end of the rib cage and the hip by using an acupuncture needling instrument as above. Needling parameters were identical to those used in human subjects above, except that pullout speed was 1 mm/s. Before inserting the acupuncture needles, we inserted a sponge through a midline abdominal incision on both sides of the peritoneal cavity next to the abdominal wall in order to prevent the acupuncture needles from penetrating abdominal organs (the material of the sponge was such that a pullout force of less than 5 g was measured when the needle was inserted and pulled out of the sponge, both with and without rotation). Right and left sides of the abdomen were needled in random order and were also randomized to either UNI or NO. The number of needle revolutions was 32 for UNI and 0 for NO. Needle insertion depth was constant at 30 mm. In all insertions, the needle went through the entire thickness of the abdominal wall. During pullout, needle retraction was stopped after the peak of pullout force at a load value corresponding to 50% of the peak, with the needle remaining in the skin. After needling of both sides and while still under anesthesia, the rat was killed by decapitation. The whole body of the animal was then immersion-fixed in 10% formalin for 24 h. After fixation, a 2 cm × 0.5 cm tissue block, including the needle, was excised. The needle track was labeled with a 1:1 mixture of India ink and polyethylene glycol. Tissue blocks were processed for histology and were serial-sectioned perpendicular to the plane of the skin (roughly parallel to the needle track) at 10-μm thickness. Every 20th section was stained with Hematoxylin/Eosin. In the rat, subcutaneous tissue is located between a thin layer of subcutaneous muscle and abdominal wall muscles. In this orientation, subcutaneous tissue appears as two fine layers of relatively dense connective tissue separated by a layer of loose adipose-rich tissue. In each section, the area occupied by dense subcutaneous connective tissue was traced within a constant 2 mm × 2 mm area centered on the needle track by using a Lucivid Image Analysis System (MicroBrightFields Inc., Colchester, VT). The relative volume of dense subcutaneous connective tissue within a fixed volume surrounding the needle was calculated as follows: volume = Σ(area) x (section thickness) x (section interval). Sections were coded so that the operator was blind to the study variable.

Preparation of rat abdominal wall tissue explants

Eight male Sprague Dawley rats (300–350 grams) were decapitated under isoflurane general anesthesia. Immediately after death, a midline abdominal incision was made through the skin from the xiphoid process to the pubic symphysis. The skin and underlying subcutaneous tissue (including subcutaneous muscle) were dissected away from abdominal wall and back muscles to

yield a 10 cm × 15 cm piece of tissue and were placed in 37° HEPES buffer, pH 7.4, containing (mM): NaCl 141.8, KCl 4.7, $MgSO_4$ 1.7, ethylene diamine tetra-acetate (EDTA) 0.39, $CaCl_2$ 2.8, N-(2-hydroxyethyl) piperazine-2'-(2-ethanesulphonic acid) (HEPES) 238.3, KH_2PO_4 1.2, glucose 5.0. Right and left sides of the sample were then assigned randomly to either UNI or NO. On each side, a circular tissue sample of 2 cm radius was excised, such that the center of the circle was at the level of the last rib and 4 cm from the middle of the back. Following excision, the tissue sample was placed, subcutaneous tissue side up, on the circular plexiglass back plate of a custom-made tissue holder. The specimen was kept irrigated with buffer. An acupuncture needle was inserted through a hole in the center of the back plate and through the center of the tissue sample, perpendicular to the plane of the skin (Fig. 2b). The number of revolutions was 32 for UNI and 0 for NO. The needle was rotated by hand at approximately two revolutions/s, and revolutions were counted visually by following a mark on the side of the needle handle. The acupuncture needle was then cut on the subcutaneous tissue side, such that the cut end of the needle was level with the edge of the tissue. The front plate of the sample holder, which included a 12-μm-thick mylar film as an acoustic window, was fitted onto the back plate and sealed with an O-ring (Fig. 2). The chamber size was adjusted so that the subcutaneous tissue made light uniform contact with the mylar film. The order of scanning was counterbalanced across the two treatment conditions (NO and UNI). Average (± SD) time from death to scanning of sample 1 was 47 ± 12 min, and from scanning of sample 1 to scanning of sample 2 was 56 ± 18 min. During these intervals, the tissue was either immersed in, or continuously irrigated with, 37° HEPES buffer.

Scanning Acoustic Microscopy

A block diagram of the scanning acoustic microscope is shown in Figure 2. A 50 MHz focusing copolymer transducer made by the Department of Biophysics, University of Toronto, Canada, was used in this study. The aperture and f-number of the transducer were, respectively, 2 mm and 2.25 mm. The transducer was driven by a 500 MHz bandwidth Pulser/Receiver (Panametrics, Model 5910PR and 5910RPP, Waltham, MA) operating in pulse-echo mode. When triggered, a short ultrasonic pulse was generated by the transducer, which also received the reflected and scattered ultrasonic pulse returning from tissue. The radio-frequency (RF) signal corresponding to the received pulse was amplified and digitized at 500 MHz and 8-bit resolution (Gage 8500 DAQ board, Montreal, Quebec, Canada).

The transducer and sample-holder were immersed in a distilled water bath at room temperature. The sample holder was held stationary, whereas the transducer was mounted on a three-axis precision motion system (Newport ESP 300, Newport Inc, Irvine, CA), which translated the transducer relative to the specimen under computer control. The *Z*-axis of the motion system was oriented perpendicular to the specimen surface. The *Z* position of the transducer was adjusted such that the ultrasound beam was focused on a tissue plane 100μm deep to the mylar window. The timing of the data collection gate was adjusted so that only echoes generated by the tissue would be collected. The characteristic sharp peaks produced by the mylar film and the back plate were rejected. The investigator performing these adjustments was blind to the study variable (UNI vs. NO). In rat abdominal wall explants, subcutaneous tissue thickness is approximately 500 μm and can increase to several millimeters with needle rotation (14). The focal area of the

transducer was therefore within subcutaneous tissue in both rotated and non-rotated samples. Once the transducer's *Z*-position was established, it was not changed during the image scan.

To generate the image, the transducer was translated in the *X*-*Y* plane (parallel to the specimen's surface) in a raster scan fashion. Every 20 μm, an ultrasound pulse was generated. Ultrasound pulsing was coordinated with the scan by a high-speed position-detector (PCI 601, National Instruments, Austin, TX), which monitored the motion stage's position encoders directly. Data acquisition and scanning were controlled by a personal computer. In all specimens, an 8 mm × 8 mm area was scanned and centered on the needle. Scanning time was 25 min per sample.

After completion of the scan, the raw RF data were processed to form the final image. Each image pixel corresponded to one ultrasound pulse. The gray level of the pixel was set to correlate linearly with the peak value of the received RF signal (echo) from that pulse. A bitmap image gray level image (400 rows by 400 columns) corresponding to 8 mm × 8 mm was thus created. Each pixel represents a tissue location measuring approximately 20 μm × 20μm and in a plane 100 μm deep to the surface contacting the mylar film.

Fourier Transform Analysis

Fourier Transform Analysis (FTA) was used to test for periodicity in the acoustic images. The image shown in Figure 5a is composed predominantly of uniform gray level dots with a relative lack of pattern. In contrast, a readily visible spiral-like pattern can be seen in Figures 5b and 6a. Testing for periodicity permits mathematical and statistical analysis of the morphological pattern observed in the images. A spiral pattern is expected to show periodicity along radial lines originating from the center of the spiral. We therefore performed the FTA in polar (ρ, θ) coordinates. For each image, the location of the acupuncture needle was estimated and taken as the origin of the coordinates, and eight lines of data were analyzed, corresponding to $\theta = 0°$, 45°, 90°, 135°, 180°, 225°, 270°, and 325°. Each line measured 3.4 mm and contained 168 data points. An investigator blind to the study variables performed the analysis by using Matlab (The MathWorks, Inc. Natick, MA) Discrete Fourier Transform software. In the spatial frequency spectrum, peaks may appear at certain spatial frequencies corresponding to certain spatial periodicities developed in an image. The frequency component with the greatest amplitude (excluding the DC component corresponding to the average gray value for that line) was identified for each line. This peak value, reflecting the dominant periodicity, was taken as the outcome measure for that line.

Statistical methods

Human subjects

Subjects were randomized to the three different needle manipulation types (NO, BI, UNI), which were analyzed separately. Repeated measures analysis of variance was used to assess differences in mean pullout force across the four needle insertion sites (Lumbar $_{D}$, Lumbar $_{D+1}$, Sacral $_{D}$, Sacral $_{D+1}$). Pairwise comparisons among means when appropriate, were performed by using Fisher's LSD. A linear contrast was constructed to test whether increased depth at the lumbar location produced greater difference in mean pullout force than that observed at the sacral

location. All data corresponding to pullout force was log transformed before analysis in order to satisfy the normality and homogeneity of variance assumptions associated with analysis of variance (18). All means presented for pullout force therefore are geometric means, which correspond to the antilog of the arithmetic means of the log-transformed data. Approximate standard errors associated with geometric means were computed based on the method described by Kendall and Stuart (19).

In vivo animal experiment

Paired *t*-tests were used to compare NO and UNI with respect to pullout force and volume measurements. Correlation analyses were used to examine the relationship between the two outcome measures.

Fourier analysis of rat tissue ultrasound images

Repeated ANOVA measures were used to evaluate the significance associated with the difference in average peak value between NO and UNI. The eight lines used to evaluate each image were considered nested within image. The F-test corresponding to differences between treatment conditions thus utilized rat *x* treatment condition (df=7) as its error term, rather than within image replication. Statistical analyses were performed by using using SAS Institute Inc. (Cary, NC) statistical software.

RESULTS

In vivo human pullout force measurements

Pullout force measurements are summarized in Table 1 and illustrated in Figure 1. With all three needle manipulation types, significant differences in mean pullout force were observed across the four needle locations (Repeated Measures ANOVA, NO: $F_{3,57}$=48.0, P<0.001; BI: $F_{3,54}$=15.7, P<0.001; UNI: $F_{3,57}$=12.7, P<0.001).

Mean pullout force at needle depth D+1 was always greater than at needle depth D. With one exception (UNI at the lumbar location), this difference was statistically significant (Fisher's LSD, P<0.05).

The difference in pullout force between the two lumbar needles Δ_L corresponded to the effect of 1 cm of muscle penetration. In contrast, the difference in pullout force between the two sacral needles Δ_S corresponded to the effect of 1 cm of subcutaneous tissue penetration (Fig. 1a). With both NO and BI, there was no evidence that Δ_L was greater than Δ_S (Linear Contrast, $F_{1,57}$=1.19, P=0.28 and $F_{1,54}$=0.03, P=0.86 for NO and BI respectively). With UNI, Δ_S was significantly greater than Δ_L, indicating that the difference in pullout force between depths D and D+1 was greater when both needles were not in muscle (Linear Contrast $F_{1,57}$=5.7, P=0.02) (Fig. 1b).

In vivo rat pullout force and connective tissue volume measurements

Mean (±SE) pullout force was 2.48±0.39 N with UNI compared with 0.17±0.01 N with NO, (paired *t*-test, t_{12}=5.9, *P*<0.001) (Fig. 3a). Histological examination of tissue sections revealed findings indistinguishable from those previously observed in rat tissue explants: we found marked thickening of dense subcutaneous connective tissue in the vicinity of the rotated needle (Fig. 4). Relative dense connective tissue volume was significantly greater with UNI (1.01±0.11mm^3) than with NO (0.5±0.06mm^3), (paired *t*-test, t_{10}=5.0, *P* < 0.001) (Fig. 3b). With UNI, pullout force and volume were positively correlated (r=0.78, *P*<0.01) (Fig. 3c), whereas no significant correlation was found with NO (r=0.47, *P*=0.14).

In vitro ultrasound imaging of rat tissue explants

Sample ultrasound images are shown in Figure 5 for NO (a) and UNI (b). In Figure 6, another sample with needle rotation is shown, imaged with both ultrasound and histology (see Appendix). The needle is visible as a black dot in the center of each ultrasound image. A spiral pattern was observed in all samples with UNI, but never with NO. In all images, the peak value yielded by the Fourier transform corresponded to a wavelength ranging from 0.2 to 1.7 mm/cycle. Mean (±SE) peak value in gray scale units was 28.7±2.2 with UNI vs. 22.0±1.4 with NO (Repeated Measures ANOVA, $F_{1,7}$=9.6, *P*=0.017) (Fig. 5c).

DISCUSSION

The results of this study strongly support connective tissue winding as the mechanism responsible for the increase in pullout force induced by needle manipulation. We found no evidence that increase needle penetration of muscle results in a greater pullout force than increased penetration of subcutaneous tissue in humans. In fact, with uni-directional needle rotation, we found the opposite: a greater increase in pullout force in subcutaneous tissue, compared with muscle. We also found in live rats that pullout force and dense connective tissue volume were both greater with uni-directional rotation than with no rotation. These results show that needle grasp can be measured in live animals, and that the connective tissue changes previously observed in animal tissue explants also occur in vivo. Finally, we found evidence that periodic patterns were developed in ultrasound images of rat subcutaneous tissue explants with uni-directional rotation, compared with no rotation. Ultrasound images of tissues are generated primarily by interfaces between tissue components such as collagen and fat (see Appendix). The spiral pattern seen in the rotated sample suggests that the increased periodic order with needle rotation is due to winding of connective tissue around the needle, which causes reorganization of tissue components relative to the needle. A mechanism involving tissue winding is consistent with previous observations in humans: uni-directional rotation was accompanied by rapidly increasing needle/tissue torque, whereas bi-directional rotation appeared to be associated with alternating winding and unwinding, with incomplete unwinding resulting in a slower and lesser torque buildup (11).

Winding of connective tissue is a mechanism with relevance not only to the field of acupuncture, but also to the fields of mechanical signal transduction and connective tissue physiology. The increase in friction force that occurs with progressive winding of material around a small

diameter shaft makes winding an ideal mechanism for achieving a tight mechanical coupling between an instrument (needle) and tissue. Achieving this mechanical coupling allows movements of the needle to deliver a powerful mechanical signal into the tissue. Cellular and molecular responses to mechanical stresses have been the subject of intense and fruitful investigations during the past decade. It has become clear that mechanical forces can be transduced across the cell membrane via the mechanical link existing at focal adhesion complexes between extracellular matrix and intracellular cytoskeleton (20). It has also been shown that cellular responses to mechanical stimuli can include cell contraction, signaling pathway activation, and gene expression (21). The great majority of studies on the effects of mechanotransduction so far have been performed in tissue culture environments. The study of the effects of mechanical forces on whole tissue is an important extension of this basic work, allowing the examination of these effects in the context of native tissue architecture. In this study, we have demonstrated that acupuncture needle rotation results in a measurable deformation of connective tissue. Pulling of collagen and/or elastic fibers and deformation of extracellular matrix during needle manipulation may have powerful and long-lasting effects on local cells, including synthesis and release of extracellular matrix components and modification of interstitial connective tissue composition (14). Such changes in matrix composition in turn potentially can modulate the effect of future mechanical signal transduction in connective tissue cells (22).

Our results have important implications for our understanding of acupuncture. For the past 30 years, a general assumption of acupuncture research has been that the therapeutic effects of acupuncture essentially take place via the nervous system (7, 23). This view was suggested by early experiments showing that the analgesic effect of acupuncture manipulation is eliminated by blocking the sensory nerve supply to deep tissues (24) and by the observation that many "acupuncture points" are located near sensory nerves and neuromuscular attachments (23, 25–27). Numerous neural effects of acupuncture treatments have since been demonstrated, such as the release of central nervous system endogenous pain-inhibitory substances (28, 29), activation of autonomic nervous system reflexes (30, 31), and changes in specific brain structures seen with fMRI (32, 33). This study, by providing evidence of subcutaneous connective tissue involvement in needle grasp, suggests that the mechanism of action of acupuncture also involves extraneural tissues and paves the way for further investigations of local cellular and molecular effects of acupuncture needle manipulation.

The results of this study also highlight the potentially important role of interstitial connective tissue in neuromodulation. Subcutaneous connective tissue forms a continuous tissue plane throughout the body. This tissue plane is itself continuous with dermis, with interstitial planes separating muscles, bones, and tendons and with intramuscular connective tissue. These connective tissue planes also constitute the "milieu" surrounding a wide variety of sensory mechanoreceptors and nociceptors (34). Techniques such as acupuncture may act not simply via neural stimulation, but also by producing changes in the connective tissue milieu surrounding sensory afferent nerve fibers. These connective tissue changes may be long lasting, which may explain claims that acupuncture can have prolonged effects.

In this study, we did not test traditionally defined "acupuncture points". The lumbar and sacral locations used in human subjects and the needling locations used in animal experiments were all

based on standardized measurements. In contrast, acupuncture points are traditionally located by using proportional measurements such as the fraction of the distance between two anatomical structures (3). The points tested in humans therefore may have coincided with acupuncture points in some subjects but not in others. We have previously reported that pullout force was on average 18% greater at acupuncture points than at corresponding "non-acupuncture" control points (11). However, the effect of needle manipulation (167% and 52% increases in pullout force for BI and UNI, respectively) was much greater in magnitude than the effect of point type (acupuncture vs. control) (11). Moreover, the previous study showed that needle manipulation significantly increased pullout force at both acupuncture points and control points. Together, these findings indicated that the phenomenon of needle grasp is present throughout the body, albeit slightly enhanced at acupuncture points. The current data, suggesting a mechanism for needle grasp involving connective tissue, are compatible with these findings because acupuncture points tend to be located along cleavage planes between muscles, or between muscle and bone or tendon (3, 35). Needle grasp may be slightly greater at acupuncture points because the needle can be inserted into slightly more connective tissue at those points.

In conclusion, the results of this study show that needle grasp is not due to a muscle contraction, and that needle rotation causes both increased pullout force and measurable changes in connective tissue architecture. Our results support the model that these biomechanical and architectural changes are due to winding of connective tissue and creation of a tight mechanical coupling between needle and tissue. Mounting evidence in the field of mechanotransduction suggests that mechanical stimuli can lead to a wide variety of cellular and extracellular events. These events may range from cell contraction to gene expression and modification of extracellular matrix composition. Connective tissue matrix deformation during acupuncture needle manipulation may therefore have prolonged and far-reaching effects. Further studies of these effects will potentially contribute to a better understanding both of acupuncture and of the effects of mechanical forces in tissues.

APPENDIX

Characteristic features of acoustic images

In general, the acoustic properties of biological tissue show greater contrast than their optical counterparts. Therefore, unlike optical images, acoustic images can be readily obtained without the need for tissue staining. The contrast of acoustic imaging is closely related to the acoustic impedance of a specimen. The acoustic impedance is defined as the product of the mass density and the speed of sound of a material. If a specimen consists of two materials A and B (A is spatially closer to a transducer than B), the acoustic wave generated by the transducer propagates in material A and impinges on the interface between A and B at near normal incidence condition. The sound wave is then partially reflected back from the interface before it reaches B. The intensity of the returned signal depends on the difference of acoustic impedance between A and B if other conditions are constant. For example, the acoustic impedances of fat, muscle, and collagen are 1360, 1640, and 1790 kg/(m^2s) respectively (36). The portions of acoustic intensity reflected back at near normal incidence are 0.19%, 0.87%, and 1.9%, respectively, for muscle/collagen, fat/muscle, and fat/collagen interfaces. Among the three interfaces, the fat/collagen interface reflects the maximum acoustic energy back to the transducer, whereas

muscle/collagen interface reflects the minimum. If the specimen is a uniform and isotropic material and has no interface, the returning signal is due to scattering from tissue and goes in all directions. Thus the scattered signal received by the transducer is small. The axial (in a direction parallel to the wave propagation) and the lateral (in a direction perpendicular to the wave propagation direction) resolutions of acoustic images generated by the system used in this study are about 60 μm and 80 μm, respectively.

In Figure 6, an acoustic image (a) and an optical histology image (b) of the same rat abdominal wall tissue explant are shown. The acoustic image was obtained by using a 0.12μs data collection gate starting from a tissue depth of 0.35 mm from the surface of the tissue specimen. The optical image was obtained by fixing the tissue sample in 10% formalin immediately after ultrasound scanning (fixed with the needle still in place and pulling the needle out after fixation), paraffin-embedding, serial-sectioning at 10-μm thickness parallel to the ultrasound scanning plane and staining the section corresponding to the tissue depth of the acoustic image with Hematoxylin/Eosin. Similarity between the acoustic and optical patterns suggests that clear acoustic interfaces correspond to areas rich in fat/collagen interfaces in the optical image.

Another observation is that the location of the acupuncture needle appears to be larger in the acoustic image than in the optical image. The needle appears black in the ultrasound image because the acoustic wave was strongly reflected by the acupuncture needle surface, which was flush with the surface of the tissue. Therefore, within the data collection gate, the signal was negligibly small. Because ultrasound was focused at a tissue depth of about 0.35 mm from the surface of the tissue specimen, the surface of the metallic needle was in front of the focal zone. This finding is consistent with the needle appearing wider in the acoustic image than its actual dimension (250 μm diameter). In the optical image, the empty hole corresponds to the location where the needle was pulled out after fixation.

ACKNOWLEDGMENTS

This study was funded by the National Institutes of Health (NIH) Center for Complementary and Alternative Medicine Grants # RO1AT00133 and R21 AT00300. The human protocol was conducted at the University of Vermont General Clinical Research Center at Fletcher Allen Health Care supported by NIH Grant # M01RR00109.

We thank Gale A. Weld for recruitment of volunteers; Gary J. Nelson and Adam D. Reisner for help with illustrations; and Robert W. Hamill, Margaret A. Vizzard, and Marilyn J. Cipolla for comments on the manuscript.

REFERENCES

1. Eisenberg, D.M., Davis, R.B., Ettner, S.L., Appel, S., Wilkey, S., Van Rompay, M., and Kessler, R.C. (1998). Trends in alternative medicine use in the United States, 1990-1997: results of a follow-up national survey. *JAMA*. 280,1569-1575

2. Anonymous. (Circa 300 B.C). *Yellow Emperor's Classic of Internal Medicine, Su Wen.* Transl: Lu HC. Vancouver: Academy of Oriental Heritage, 1994.

3. Cheng X. (1987). *Chinese Acupuncture and Moxibustion*. Foreign Language Press, Beijing.

4. NIH Consensus Statement. (1997). *Acupuncture*. 15,1-34.

5. Shanghai College of Traditional Medicine. (1987). *Acupuncture, A Comprehensive Text*. Transl. O'Connor J, Bensky D. Eastland Press, Seattle.

6. Denmei, S. (1990). *Introduction to Meridian Therapy: Classical Japanese Acupuncture*. Eastland Press, Seattle.

7. Stux, G., and Pomeranz, B. (1995). *Basics of Acupuncture*. 3rd ed. Springer-Verlag, Berlin.

8. Helms, J.M. (1995). *Acupuncture Energetics-A Clinical Approach for Physicians*. Medical Acupuncture Publishers, Berkeley.

9. Soulie de Morant, G. (1994). *Chinese Acupuncture*. English ed. Paradigm Publications, Brookline.

10. Yang, J. (1601). *The Golden Needle and Other Odes of Traditional Acupuncture,* 1601. Transl. by Bertschinger R. (1991), Churchill Livingstone, Edinburgh.

11. Langevin, H.M., Churchill, D.L., Fox, J.R., Badger, G.J., Garra, B.S., and Krag, M.H. (2001). Biomechanical response to acupuncture needling in humans. *J Appl Physiol.* 91,2471-2478.

12. Shanghai Institute of Physiology. (1973). Electromyographic activity produced locally by acupuncture manipulation. (In Chinese) *Chin Med J* 153,532-535.

13. Gunn, C.C., and Milbrandt, W.E. (1977). The neurological mechanism of needle grasp in acupuncture. *Am J Acup* 5,115-120.

14. Langevin, H.M., Churchill, D.L., and Cipolla, M.J. (2001). Mechanical signaling through connective tissue: a mechanism for the therapeutic effect of acupuncture. *FASEB J* 15,2275-2282.

15. Kimura, M., Tohya, K., Kuroiwa, K., Oda, H., Gorawski, E.C., Hua, Z.X., Toda, S., Ohnishi, M., and Noguchi, E. (1992). Electron microscopical and immunohistochemical studies on the induction of 'qi' employing needling manipulation. *Am J Chin Med* 20,25-35.

16. Hibbeler, R.C. (1995) *Engineering Mechanics–Statics and Dynamics*, Prentice-Hall, Englewood Cliffs, N.J.

17. Briggs, A. (1992). *Acoustic Microscopy*, Clarendon Press, Oxford.

18. Box, G.E.P., Hunter, W.G., and Hunter, J.S. (1978). *Statistics for Experimenters*. John Wiley& Sons, New York.

19. Kendall, M.G., and Stuart, A. (1969). *The Advanced Theory of Statistics* Vol. 1. Charles Griffin and Co, London.

20. Schwartz, M.A., and Ingber, D.E. (1994) Integrating with integrins. *Molec Biol Cell.* 5,389-393.

21. Banes, A.J., Tsuzaki, M., Yamamoto, J., Fischer, T., Brigman, B., Brown, T. and Miller, M. (1995). Mechanoreception at the cellular level: the detection, interpretation and diversity of responses to mechanical signals. *Biochem Cell Biol.*73,349-365.

22. Brand, R.A. (1997). What do tissues and cells know of mechanics? *Ann Med.*29,267-269.

23. Ulett, G.A., Han, S., and Han, J.S. (1998). Electroacupuncture: mechanisms and clinical applications. *Biol Psych.* 44,129-138.

24. Chiang, C.Y., Chang, C.T., Chu, H.L., and Yang, L.F. (1973). Peripheral afferent pathway for acupuncture analgesia. *Sci Sin.* 16,210-217.

25. Dung, H.C. (1984). Anatomical features contributing to the formation of acupuncture points. *Am J Acup.* 12,139-143.

26. Gunn, C.C., Ditchburn, F.G., King, M.H., and Renwick, G.J. (1976). Acupuncture loci: a proposal for their classification according to their relationship to known neural structures. *Am J Chin Med.* 4,183-195.

27. Liu, K.Y., Varela, M., and Oswald, R. (1975). The correspondence between some motor points and acupuncture loci. *Am J Chin Med.* 3,347-358.

28. Han, J.S. (1987). *The Neurochemical Basis of Pain Relief by Acupuncture*. Chinese and Medical Science Technology Press, Beijing.

29. Pomeranz, B., and Chiu, D. (1976). Naloxone blocks acupuncture analgesia and causes hyperalgesia: endorphin is implicated. *Life Sci.* 19,1757-1762.

30. Andersson, S. (1993). The functional background in acupuncture effects. *Scand. J. Rehab. Med. Suppl.* 29,31-60.

31. Ernst, M., and Lee, M.H.M. (1985). Sympathetic vasomotor changes induced by manual and electrical acupuncture of the Hoku point visualized by thermography. *Pain* 21,25-33.

32. Cho, Z.H., Chung, S.C., Jones, J.O., Parks, H.J., Lee, H.J., Wong, E.K., and Min, B.I. (1998). New findings of the correlation between acupoints and corresponding brain cortices using functional MRI. *Proc Natl Acad Sci USA* 95,2670-2673.

33. Hui, K.S., Liu, J., Makris, N., Gollub, R.L., Chen, A.J.W., Moore, C.I., Kennedy, D.N., Rosen, B.R., and Kwong, K.K. (2000). Acupuncture modulates the limbic system and subcortical gray structures of the human brain: evidence from fMRI studies in normal subjects. *Human Brain Mapping* 9,13-25.

34. Willis, W.D. and Coggeshall, R.E. (1991) *Sensory Mechanisms of the Spinal Cord*, Plenum Press, New York

35. Worsley, J.R. (1982). *Traditional Chinese Acupuncture Volume 1: Meridians and points*. Element Books, Tisbury, U.K.

36. Duck, F.A. (1990). *Physical Properties of Tissue*, Academic Press, London.

Received November 30, 2001; revised February 20, 2002.

Table 1

Pullout force measurements with varying needle depth.

Needle manipulation type	Lumbar $_{D}$	Lumbar $_{D+1}$	Sacral $_{D}$	Sacral $_{D+1}$
No manipulation	$0.2 \pm .01^{c}$	0.42 ± 0.02^{a}	0.18 ± 0.0^{c}	0.32 ± 0.02^{b}
Bidirectional rotation	0.4 ± 0.06^{b}	0.82 ± 0.10^{a}	0.35 ± 0.06^{b}	0.75 ± 0.07^{a}
Unidirectional rotation	$0.67 \pm 0.18^{b, c}$	1.1 ± 0.21^{b}	0.62 ± 0.14^{c}	2.6 ± 0.47^{a}

Note: Pullout force measurements are in Newtons. Tabled values are mean ± SE.
Means sharing a common letter are not significantly different within each row (i.e., within needle manipulation type.)

Fig. 1

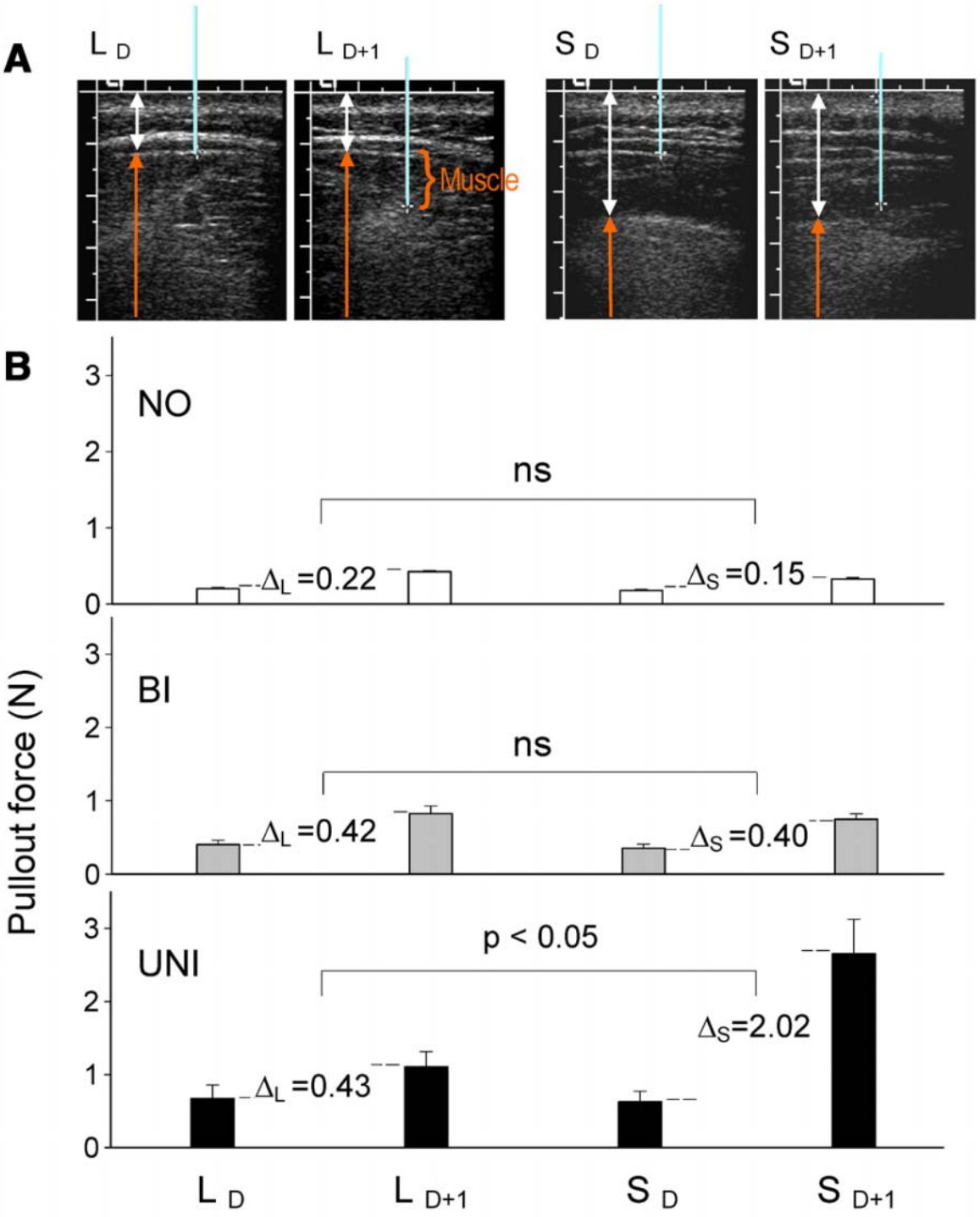

Figure 1. Pullout force measurements in humans. A) Sample ultrasound images for lumbar and sacral needling locations bilaterally. Red arrows indicate muscle, and white arrows indicate subcutaneous tissue. In each image, an acupuncture needle (drawn in blue) indicates depth of needle insertion. At the lumbar location, needle L_D was inserted to the perimuscular fascia. On the contralateral side, needle L_{D+1} was inserted 1 cm beyond the perimuscular fascia (i.e., into muscle). At the sacral location, needles S_D and S_{D+1} were inserted to the same depths as needles L_D and L_{D+1}, respectively. Because subcutaneous tissue thickness was at least 1 cm greater at the sacral than at the lumbar location in all subjects, neither needle S_D nor needle S_{D+1} penetrated muscle. **B)** Mean (± SE) pullout force with no needle rotation (NO), bidirectional needle rotation (BI) and unidirectional needle rotation (UNI). Δ_L indicates difference in pullout force between the two lumbar needles, and Δ_S the difference between the two sacral needles. Pullout force results are expressed in Newtons (N).

Fig. 2

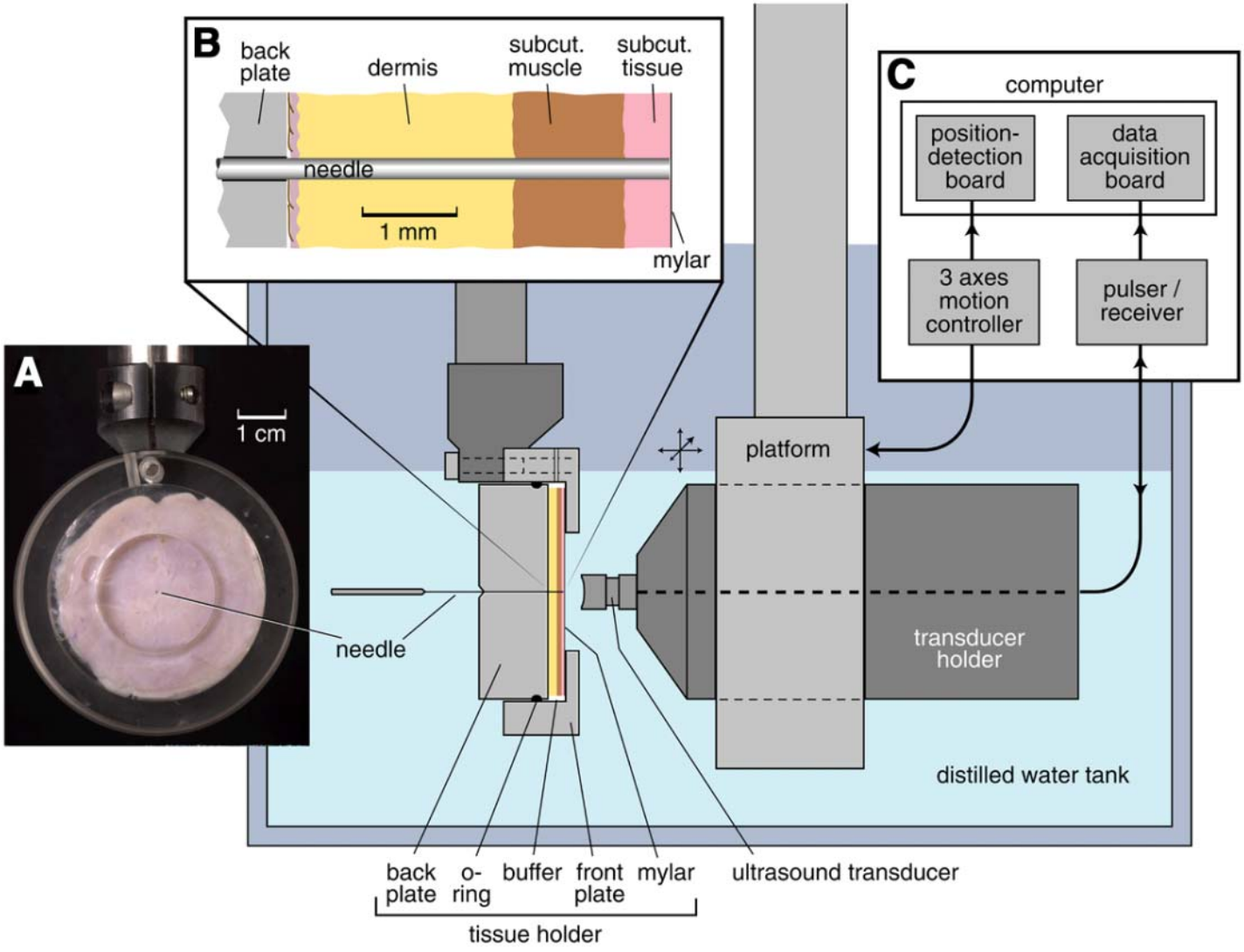

Figure 2. Ultrasound scanning acoustic microscopy system. Schematic representation of tissue sample holder and ultrasound transducer during use (side view). **A)** Tissue holder with tissue sample in place (front view); **(B)** expanded view of tissue layers through which the needle is inserted; **(C)** block diagram of system components.

Fig. 3

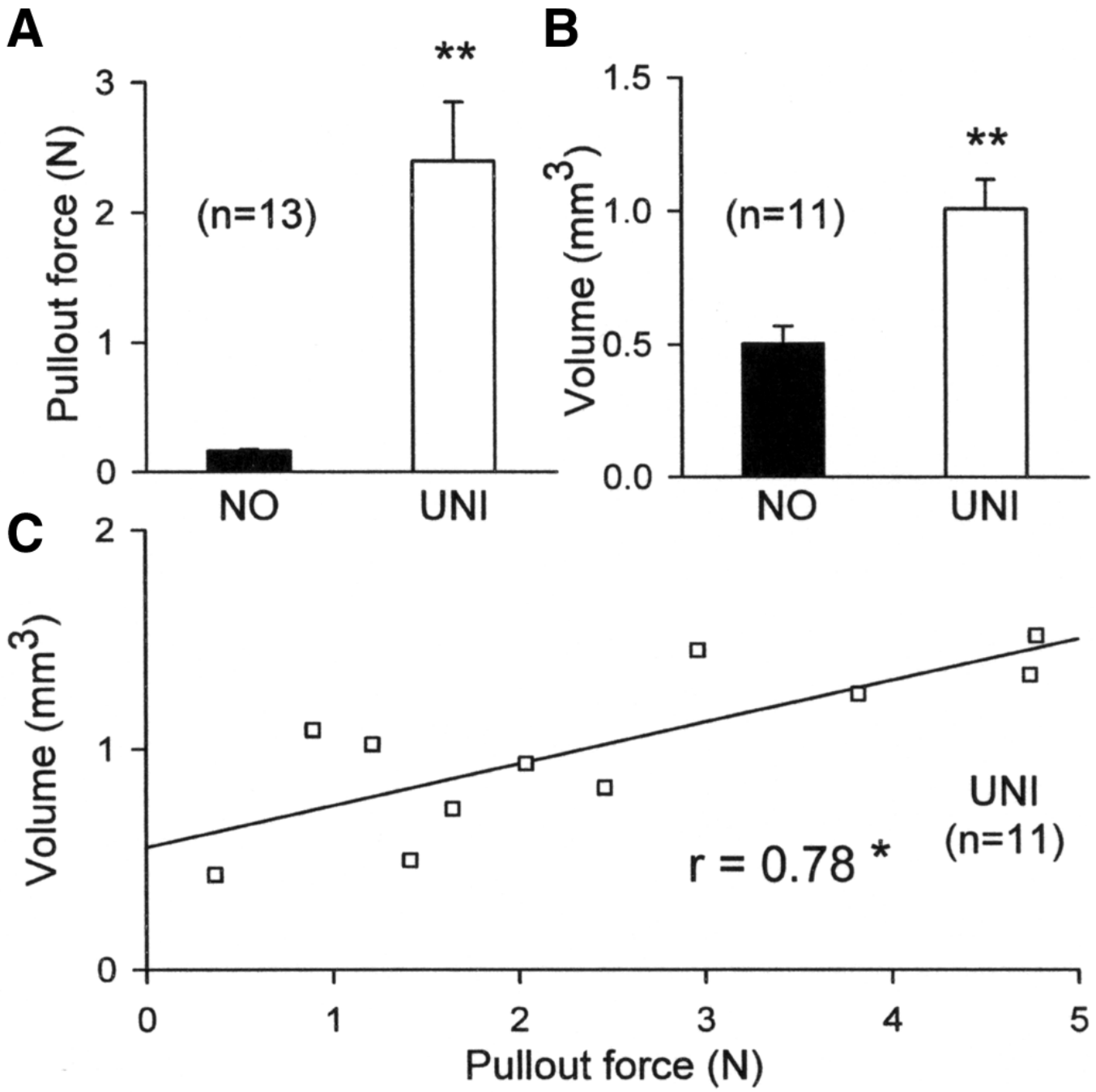

Figure 3. Rat pullout force and tissue volume measurements. Mean pullout force **(A)** and relative dense connective tissue volume **(B)** were greater with unidirectional needle rotation (UNI) than with no rotation (NO). Data shown are mean ± SE, $^{**}P<0.001$. **C)** With UNI, pullout force and volume measurements were positively correlated, $^{*}P<0.01$. Pullout force results are expressed in Newtons (N).

Fig. 4

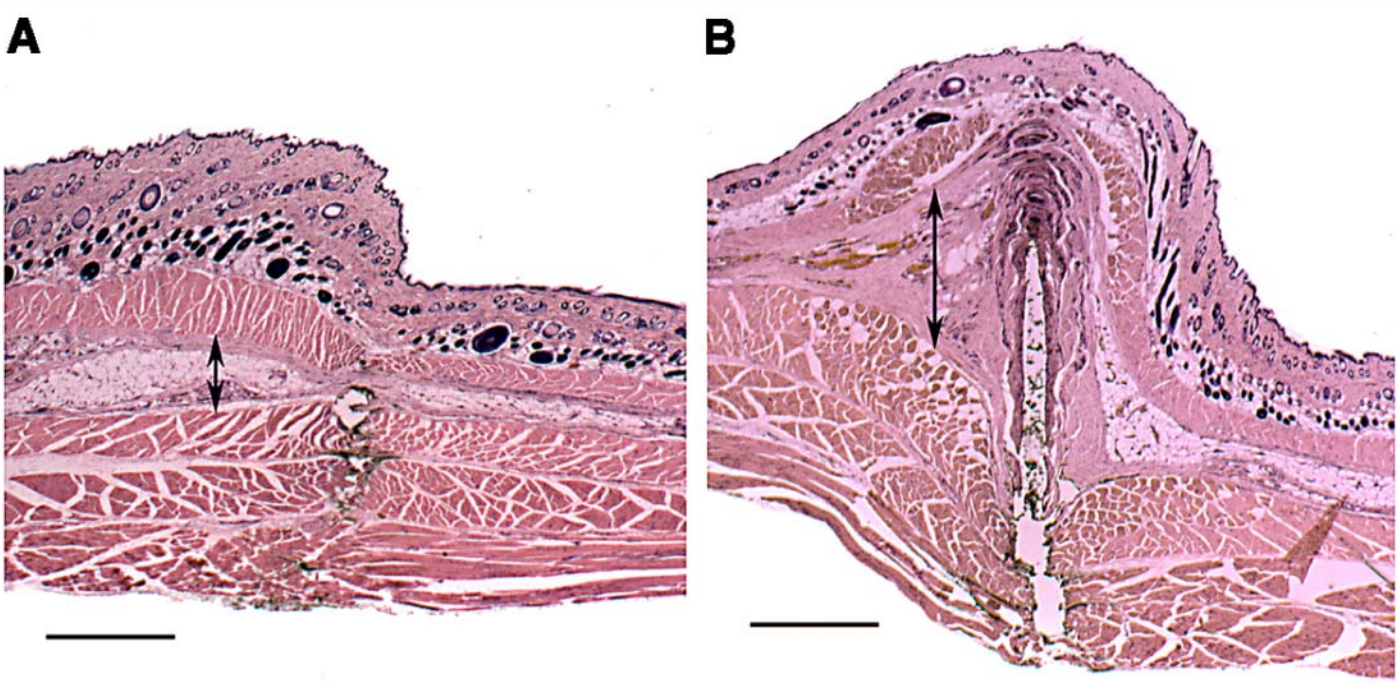

Figure 4. Rat abdominal wall tissue histology. An acupuncture needle was inserted into the abdominal wall of live anesthetized rats, followed by no rotation **(A)** or unidirectional rotation **(B)**. Immediately after needling, the animal was killed, tissues were formalin-fixed, sectioned roughly parallel to the needle track (labeled with ink), and stained with Hematoxylin/Eosin. Abdominal wall layers include dermis, subcutaneous muscle, subcutaneous tissue (arrow), and abdominal wall muscle. Marked thickening of subcutaneous tissue is seen with needle rotation. Scale bars, 1 mm.

Fig. 5

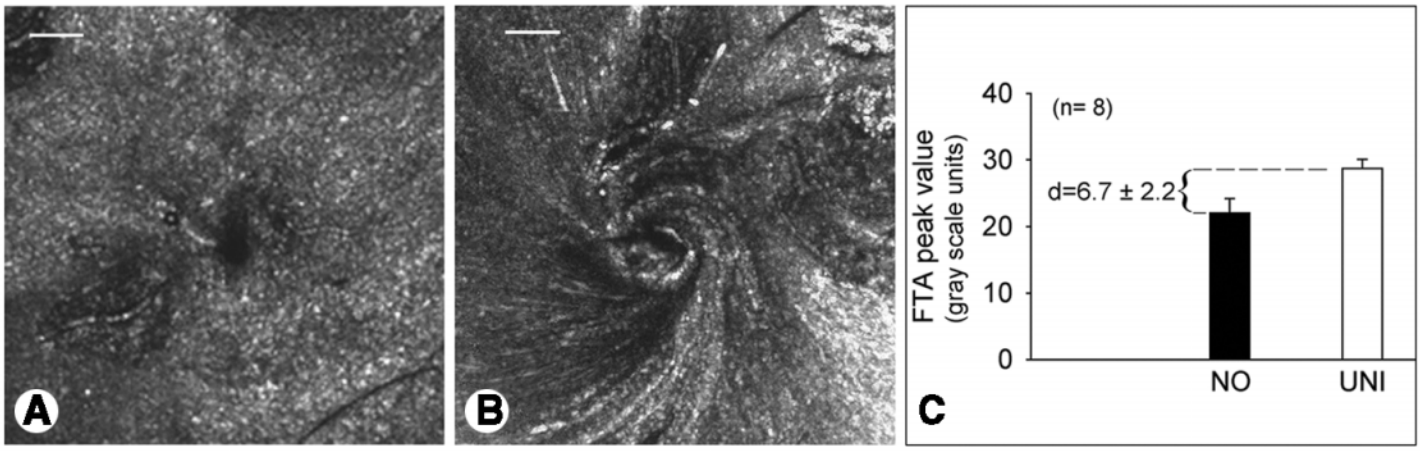

Figure 5. Ultrasound scanning acoustic microscopy of rat subcutaneous tissue. **A)** No needle rotation; **(B)** unidirectional needle rotation. The plane of ultrasound scanning is parallel to the subcutaneous tissue plane, and the needle (appearing as a black dot in the center of each image) is perpendicular to the tissue. Scale bars: 1 mm. **C)** Fourier transform analysis (FTA) of radial scan lines centered on the needle showing mean Fourier transform peak value with no rotation (NO) and unidirectional rotation (UNI). * $P<0.02$. Error bars represent SE. d Indicates the mean ± SE of the differences between sample pairs.

Fig. 6

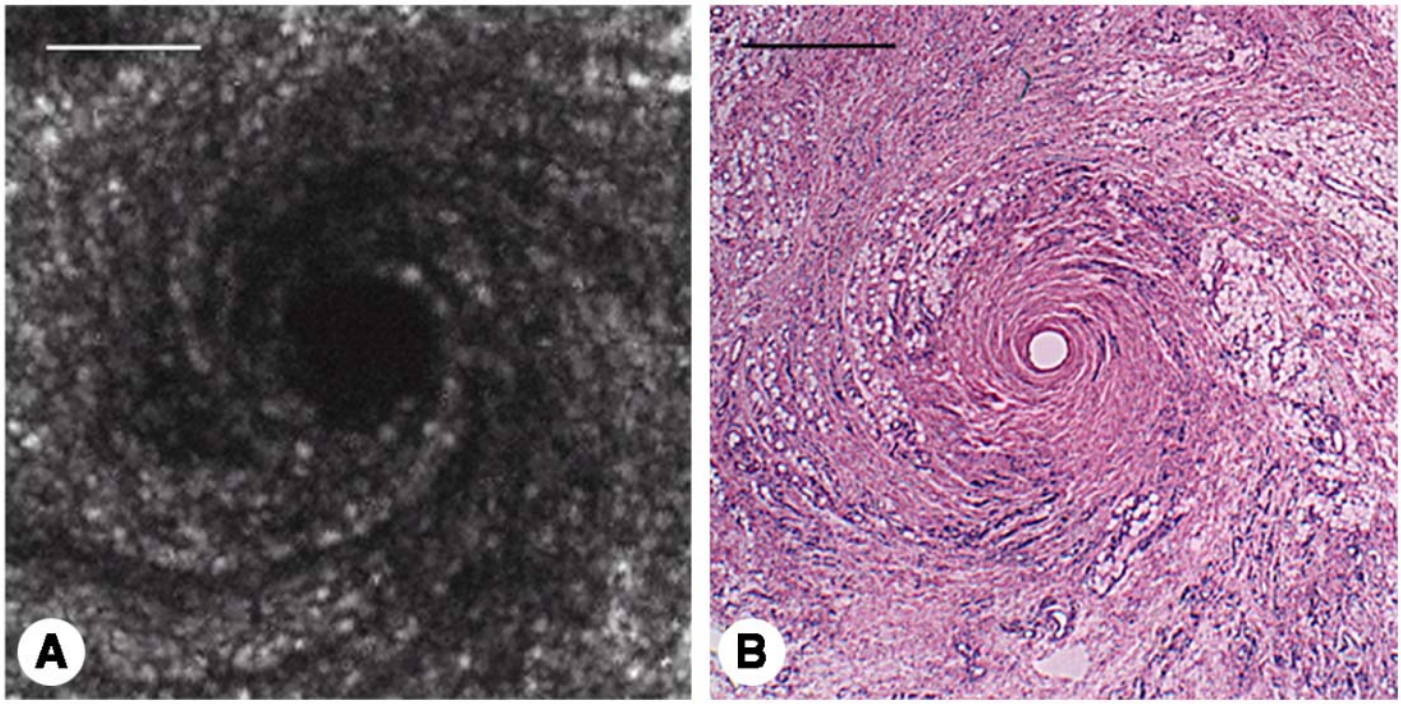

Figure 6. Acoustic and optical images of subcutaneous tissue with unidirectional needle rotation. A) Fresh tissue sample imaged with ultrasound scanning acoustic microscopy; (**B**) the same tissue sample was formalin-fixed after ultrasound imaging, embedded in paraffin, sectioned, and stained for histology with Hematoxylin/Eosin. Scale bars: 1 mm.